

REPRESENTATION OF COLORED IMAGES BY MANIFOLDS EMBEDDED IN HIGHER DIMENSIONAL NON-EUCLIDEAN SPACE

Nir Sochen and Yehoshua Y. Zeevi

Faculty of Electrical Engineering
Technion – The Technology Institute of Israel
Technion City, Haifa, 32000, ISRAEL
sochen, zeevi@ee.technion.ac.il

ABSTRACT

In image analysis, processing and understanding, it is highly desirable to process the image and feature domains by methods that are specific to these domains. We show how the geometrical framework for scale-space flows is most convenient for this purpose, and demonstrate, as an example, how one can switch continuously between different processing flows of images and color domains. The parameter that interpolates between the norms is the luminance strength, taken here as a local function of the image embedding space. The resulting spatial and/or luminance preserving flow can be used for conditional denoising, enhancement and segmentation. This example demonstrates that the proposed framework can incorporate context or task dependent data, furnished by either the human user or by an active vision subsystem, in a coherent and convenient way.

1. INTRODUCTION

In a variety of applications of denoising, smoothing, segmentation and enhancement of images, it is advantageous to have simple and automatic “buttons” that can control local smoothing of feature spaces according to some *a priori* knowledge of the task at hand. We present and implement a method that employs the recently proposed geometrical framework for nonlinear scale-space methods [2]. According to this framework, an image is treated as an embedding of a manifold in a higher dimensional manifold. A color image is accordingly considered as a two-dimensional surface **embedded** in the five-dimensional space whose coordinates are (x, y, R, G, B) .

It was suggested [2] that the nonlinear scale-space can be treated as a gradient descent with respect to a functional integral that depends on the geometry (i.e. the metric) of the image surface, as well as on the embedding and the geometry of the embedding space. In

the examples treated previously, it was assumed that the embedding space is Euclidean, and that the system of coordinates that describes it, is Cartesian [2], [3]. In fact, the geometry of the embedding space is flexible and can be determined according to the high level task that one has in mind. We view the geometry of the embedding space as the interface between the high-level task and the low-level process to be implemented.

The simplest and most intuitive example, of an adaptive smoothing of a grey-level image according to different illumination conditions, was recently achieved by having an intensity dependent embedding space geometry [6]. In this study we generalize this technique to colored images and to cases where different noise is encountered in different color channels. A different PDE algorithm was tried in [1], but with no coupling between the different color channels.

2. THE INDUCED METRIC

It is advantageous to treat images as an embedding maps. In this approach a two-dimensional image is a Riemannian surface embedded in a higher dimensional Riemannian manifold which is called the feature-spatial manifold. Let introduce on the non-linear surface a local coordinate system (σ^1, σ^2) . The embedding of this surface in, say, a three-dimensional space is done by specifying, for each point of the surface, the three-dimensional coordinates, namely:

$$(X^1(\sigma^1, \sigma^2), X^2(\sigma^1, \sigma^2), X^3(\sigma^1, \sigma^2)).$$

We introduce a one-parameter family of embedded images $(X^i(\sigma^1, \sigma^2; t))_{i=1}^3$, where t is the evolution independent variable which is called the scale or “time”. This parameter determines the degree of blurring or denoising of the image. From a geometrical viewpoint this family of embedded images describes a flow of a two-dimensional surface inside a higher dimensional space.

For a detail study of the subject we introduce some technical tools.

A fundamental concept related to Riemannian differential geometry is distance. The basic question in this context is how to measure distances? consider first the important example $\mathbf{X} : \Sigma \rightarrow \mathbb{R}^3$, where the map \mathbf{X} is explicitly given by $(X^1(\sigma^1, \sigma^2), X^2(\sigma^1, \sigma^2), X^3(\sigma^1, \sigma^2))$, and the local coordinates on the two-dimensional manifold Σ are denoted by (σ^1, σ^2) . These are analogous to arc length in the case of the one-dimensional manifold, i.e. a curve. see Fig. 1.

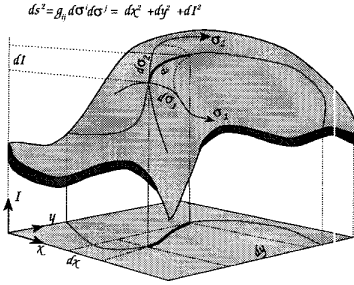


Figure 1: A diagram illustrating the local coordinate system. The line element of a surface curve ds , may be defined either as a function of a local metric of the surface (σ_1, σ_2) , or as a function of the coordinates of the embedding space (x, y, I) .

Since the local coordinates σ^i are curvilinear, the squared distance is given by a positive definite symmetric bilinear form, called the *metric*, whose components are denoted by $g_{\mu\nu}(\sigma^1, \sigma^2)$:

$$ds^2 = g_{\mu\nu} d\sigma^\mu d\sigma^\nu \equiv g_{11}(d\sigma^1)^2 + 2g_{12}d\sigma^1 d\sigma^2 + g_{22}(d\sigma^2)^2,$$

where we used Einstein summation convention in the second equality. We will denote the inverse of the metric by $g^{\mu\nu}$, so that $g^{\mu\nu}g_{\nu\gamma} = \delta_\gamma^\mu$, where δ_γ^μ is the Kronecker delta. We choose to work with the induced metric

$$g_{\mu\nu}(\sigma^1, \sigma^2) = h_{ij}(\mathbf{X})\partial_\mu X^i \partial_\nu X^j, \quad (1)$$

where $i, j = 1, \dots, \dim M$ are being summed over, and $\partial_\mu X^i \equiv \frac{\partial X^i(\sigma^1, \sigma^2)}{\partial \sigma^\mu}$.

Take for example a grey level image which is, from our viewpoint, the embedding of a surface described as a graph in \mathbb{R}^3 :

$$\mathbf{X} : (\sigma^1, \sigma^2) \rightarrow (x = \sigma^1, y = \sigma^2, z = I(\sigma^1, \sigma^2)),$$

where (x, y, z) are Cartesian coordinates. Using Eq. (1), we get

$$(g_{\mu\nu}) = \begin{pmatrix} 1 + I_x^2 & I_x I_y \\ I_x I_y & 1 + I_y^2 \end{pmatrix}, \quad (2)$$

where we used the identification $x \equiv \sigma^1$ and $y \equiv \sigma^2$ in the map \mathbf{X} . Actually, we can understand this result intuitively: Eq. (1) indicates that the distance measured on the surface by the local coordinates is equal to the distance measured in the embedding coordinates (see Fig. 1). The chain rule, then, yields the right result

$$\begin{aligned} ds^2 &= dx^2 + dy^2 + dI^2 \\ &= dx^2 + dy^2 + (I_x dx + I_y dy)^2 \\ &= (1 + I_x^2)dx^2 + 2I_x I_y dx dy + (1 + I_y^2)dy^2. \end{aligned}$$

3. COLOR SPACE COORDINATES

Two questions should be addressed in the process of generalizing the above for color images. The first relates to the variables (or coordinates), and the second to the geometry of the color space. Since the basic colors red, green and blue are correlated in most images, we adopt the Wolf-Ginosar-Zeevi approach [5] and apply the KLT to obtain an uncorrelated basis k_1, k_2 and k_3 . Denote I^a the three color planes where $a = r, g, b$. The autocorrelation matrix is

$$\Phi^{ab} = \frac{1}{NM} \sum_{i=1}^N \sum_{j=1}^M I_{ij}^a I_{ij}^b$$

The K_i s are the eigenvectors of this matrix. The autocorrelation matrix was in fact found for the family of outdoors scenes in [5] and is given explicitly by:

$$\begin{pmatrix} k_1 \\ k_2 \\ k_3 \end{pmatrix} = \begin{pmatrix} 0.3744 & 0.4452 & 0.8103 \\ -0.3249 & -0.1195 & 0.0753 \\ 0.0051 & 0.0012 & 0.0002 \end{pmatrix} \begin{pmatrix} R \\ G \\ B \end{pmatrix}. \quad (3)$$

The coordinates we use are (after defining $x = \sigma^1$ and $y = \sigma^2$)

$$(x, y, k_1(x, y), k_2(x, y), k_3(x, y)) \quad (4)$$

The k_1 coordinate represents the achromatic channel of luminance, while k_2 and k_3 are chromatic channels.

For the geometry we choose the following metric

$$ds^2 = dx^2 + dy^2 + \beta^2(k_1)dk_1^2 + c_1 dk_2^2 + c_2 dk_3^2, \quad (5)$$

where β^2 is a local function of k_1 and c_1 and c_2 are constants that take care of the dimensions. Equivalently we can say that the metric of the embedding space is

$$(h_{ij}) = \begin{pmatrix} 1 & 0 & 0 & 0 & 0 \\ 0 & 1 & 0 & 0 & 0 \\ 0 & 0 & \beta(k_1)^2 & 0 & 0 \\ 0 & 0 & 0 & 1 & 0 \\ 0 & 0 & 0 & 0 & 1 \end{pmatrix}. \quad (6)$$

The induced metric elements are according to Eq. (1):

$$\begin{aligned} g_{11} &= 1 + \beta^2(k_1)_x^2 + (k_2)_x^2 + (k_3)_x^2 \\ g_{12} &= g_{21} = \beta^2(k_1)_x(k_1)_y + (k_2)_x(k_2)_y \\ g_{22} &= 1 + \beta^2(k_1)_y^2 + (k_2)_y^2 + (k_3)_y^2. \end{aligned} \quad (7)$$

Note also that the two-dimensional image induced metric is different from the one we had in the Euclidean case.

4. THE MEASURE ON MAPS AND THE MODIFIED GRADIENT DESCENT

We use the diffusion equation which is derived as a gradient descent of an action functional. The functional in question depends on *both* the image manifold and the embedding space. Denoting by $(\Sigma, (g_{\mu\nu}))$ the image manifold and its metric and by $(M, (h_{ij}))$ the space-feature manifold and its metric, the map $\mathbf{X} : \Sigma \rightarrow M$ has the following weight [4]:

$$S[X^i, g_{\mu\nu}, h_{ij}] = \int d^m \sigma \sqrt{g} g^{\mu\nu} \partial_\mu X^i \partial_\nu X^j h_{ij}(\mathbf{X}),$$

where m is the dimension of Σ , g is the determinant of the image metric and $g^{\mu\nu}$ is the inverse of the image metric. The range of indices is $\mu, \nu = 1, \dots, \dim \Sigma$, and $i, j = 1, \dots, \dim M$. The metric of the embedding space is h_{ij} .

Using standard methods in calculus of variations, the Euler-Lagrange (EL) equations, with respect to the embedding, are (see [2] for derivation):

$$-\frac{1}{2\sqrt{g}} h^{il} \frac{\delta S}{\delta X^l} = \frac{1}{\sqrt{g}} \partial_\mu (\sqrt{g} g^{\mu\nu} \partial_\nu X^i) + \Gamma_{jk}^i \partial_\mu X^j \partial_\nu X^k g^{\mu\nu}, \quad (8)$$

where Γ_{jk}^i are the Levi-Civita connection coefficients with respect to the metric h_{ij} (defined in Eq. 11), that describes the geometry of the embedding space.

We view a scale-space as the gradient descent:

$$X_t^i \equiv \frac{\partial X^i}{\partial t} = -\frac{1}{2\sqrt{g}} h^{il} \frac{\delta S}{\delta X^l}.$$

A few remarks are in order. First, note that we used our freedom to multiply the Euler-Lagrange equations by a strictly positive function and a positive definite matrix.

This factor is the simplest one that does not change the minimization solution, while giving a reparameterization invariant expression. This choice guarantees that the flow is geometric and does not depend on the parameterization. The operator that is acting on X^i in

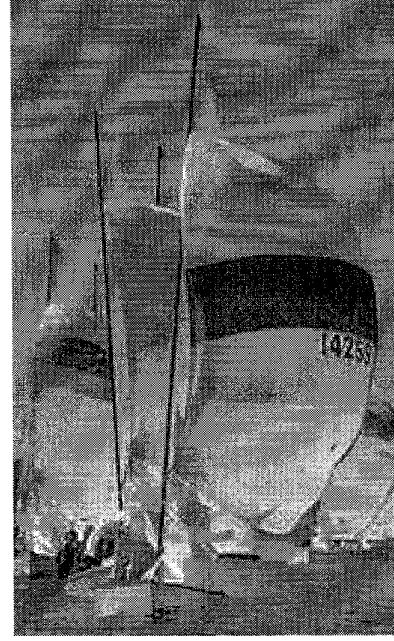


Figure 2: Original image. The sailboats image was constructed from a CCD camera by a de-mosaicing algorithm.

the first term of Eq. (8) is the natural generalization of the Laplacian from flat spaces to manifolds. It is called the Laplace-Beltrami operator, or in short *Beltrami operator*, denoted by Δ_g . In our case we get

$$\begin{aligned} \Delta_g k_i &= \left(\frac{g_x}{g} g^{11} + g_x^{11} + g_y^{12} + \frac{g_y}{g} g^{12} \right) k_{ix} \\ &= \left(\frac{g_x}{g} g^{12} + g_x^{12} + g_y^{22} + \frac{g_y}{g} g^{22} \right) k_{iy}. \end{aligned} \quad (9)$$

When the embedding is in a Euclidean space with Cartesian coordinate system, the connection elements are zero. If the embedding space is not Euclidean, we have to include the Levi-Civita coefficients, since they are not identically zero any more.

We choose a luminance normalization function $\beta(k_1)$, such that for high luminance regions β is large and the flow is less diffusive, while for low luminous regions β is small and the flow is diffusive. There are many reasonable choices for the function β . We will use for the sake of illustration only

$$\beta(k_1) = A(\tanh(a(k_1 - b)) + 1), \quad (10)$$

with A , a and b constants to be defined.

The Levi-Civita coefficients are defined as follows:

$$\Gamma_{jk}^i = \frac{1}{2} h^{il} (\partial_j h_{lk} + \partial_k h_{jl} - \partial_l h_{jk}), \quad (11)$$



Figure 3: The sailboats image smoothed by a Gaussian filtering kernel.

where there is an implicit sum over l . In our case h_{ij} is given in Eq. (6) and, using the above definition, we get

$$\Gamma_{11}^1 = \beta^{-1} \partial_{k_1} \beta = \frac{2a}{e^{2a(k_1-b)} + 1}, \quad (12)$$

where all the other coefficients vanish. The second term of Eq. (8) now reads

$$\Gamma_{ij}^1 \partial_\mu X^i \partial_\nu X^j g^{\mu\nu} = \Gamma_{11}^1 (g^{11} k_{1x}^2 + 2g^{12} k_{1x} k_{1y} + g^{22} k_{1y}^2).$$

Collecting all the terms we get the flow

$$\begin{aligned} k_{1t} &= \Delta_{g(\beta)} k_1 + \Gamma_{11}^1 (g^{11} k_{1x}^2 + 2g^{12} k_{1x} k_{1y} + g^{22} k_{1y}^2) \\ k_{2t} &= \Delta_{g(\beta)} k_2 \\ k_{3t} &= \Delta_{g(\beta)} k_3. \end{aligned} \quad (13)$$

We may choose also to work directly with the R,G,B planes and get the equivalent, but more cumbersome, equations.

5. EXPERIMENTAL RESULTS

Our algorithm is demonstrated by using the sailboats image (Fig. 2). This is a color image that was constructed from a CCD camera by a de-mosaicing algorithm. Artifacts were created in the process of de-mosaicing and we wish to filter them out. The colored images could not be included in these proceedings for



Figure 4: The sailboats image differentially smoothed by the Beltrami flow.

technical reasons. They can be viewed on the web site: <http://www-ee.technion.ac.il/users/zeevi/zeevi.html>.

Using a low pass filter i.e. convolution with a Gaussian (or equivalently solving the heat equation for each channel separately) is demonstrated in Fig. 3. This filter does not preserve sharp edges and blur the image severely. We thus need an edge preserving flow i.e. the Beltrami flow (see Fig. 4). While this is a much better result than the linear one, it still suffers from a drawback. When we look closely on the poles, we see that instead of linear objects we get a piecewise linear objects with very large and noticeable dislocations. These are artifacts of the compression that the Beltrami flow detects as a “true” edges and does not smooth out.

We therefore need is an algorithm that will smooth the structure along the poles in a manner that a linear filter does, but will smooth everything else according to the Beltrami flow. Our solution consists of using a non Euclidean space-feature whose metric is described through the Beta function which is very small for dark regions (i.e. $k_1 \approx 0$ or $R + G + B \approx 0$) and close to 1 in other places. Specifically we choose

$$\beta(k_1) = A(\tanh(a(\tilde{k}_1 - b)) + 1), \quad (14)$$

with $A = 0.5$, $a = 0.05$ and $b = 10$. We extract β from a linearly smoothed image in order to have a smooth transition between regions with high and low values of



Figure 5: The sailboats image adaptively smoothed by our algorithm.

β . The image was smoothed by 5 iterations for the linear heat equation with time step of $dt = 0.1$. The result after one iteration of our highly non-linear flow with $dt = 0.05$ is presented in Fig. 5. A closer comparison of the poles between the Beltrami flow and our algorithm is depicted in Fig. 6.

6. FURTHER EXTENSIONS OF THE PROPOSED APPROACH

The research concerned with image processing and analysis by changing the geometry of the embedding space is only in its infancy. We presented in this paper only preliminary results which demonstrate the principles in the context of a simple setting. More realistic applications require further work in order to understand, by a combination of analytical and experimental methods, the right geometry of the embedding space which is appropriate for a given task. Other potential extensions may incorporate texture, depth and various invariance properties. These questions as well as application to medical images are under current investigation.

Acknowledgments

We would like to thank R. Kimmel for useful discussions, and help in the numerical implantation. This research has been supported in part by the Ollendorff Center, the Fund for Promotion of Research at the

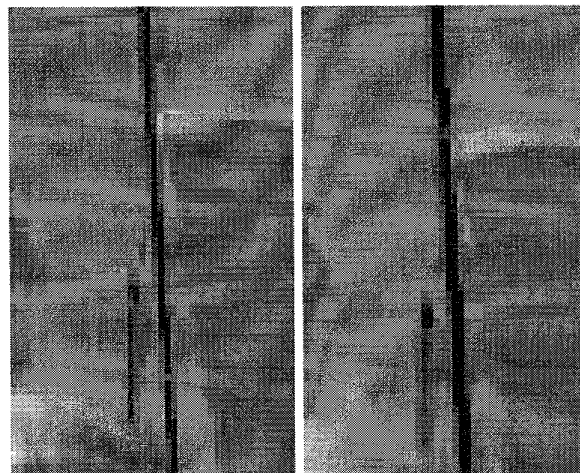


Figure 6: Comparison of the two smoothing algorithms illustrating their effects on the structure of the pole left: an enlarged part of the Beltrami smoothed image, right: An enlarged part of the image after our adaptive smoothing.

Technion, and by the Ministry of Science Vision Platform Project.

7. REFERENCES

- [1] J Kacur and K Mikula. Slow and fast diffusion effects in image processing- approximation schemes and numerical experiments. preprint no. 96-26, IWR, Heidelberg University, Germany, April 1996.
- [2] N Sochen R Kimmel and R Malladi. A general framework for low level vision. *IEEE trans. IP*, 1997, in press.
- [3] R Kimmel R Malladi and N Sochen. Images as embedded maps and minimal surfaces: Movies, color, texture, and volumetric medical images. LBNL ,UC and TAUHEP Report LBNL-40490, UC-405, Lawrence Berkeley National Laboratory, UC Berkeley and the University of Tel-Aviv, June 1997.
- [4] A M Polyakov. Quantum geometry of bosonic strings. *Physics Letters*, 103B:207, 1981.
- [5] R. Ginosar S. G. Wolf and Y. Y. Zeevi. Spatiochromatic model for colour image enhancement. The Technion CC report 186, January 1997.
- [6] N. Sochen and Y. Y. Zeevi. Representation of images by surfaces and higher dimensional manifolds in non-euclidean space. In "Curves and Surfaces 97", 1997.